

Using Vessel-Based LIDAR to Quantify Coastal Erosion during El Niño and Inter-El Niño Periods in Monterey Bay, California

Steven Quan[†], Rikk G. Kvitck[†], Douglas P. Smith[†], and Gary B. Griggs[‡]



www.cerf-jcr.org

[†]Seafloor Mapping Lab
Division of Science and Environmental Policy
California State University Monterey Bay
100 Campus Center
Seaside, CA 93955, U.S.A.
squan@csUMB.edu

[‡]Earth and Planetary Sciences Department
and Institute of Marine Sciences
University of California Santa Cruz
1156 High Street
Santa Cruz, CA 95064, U.S.A.

ABSTRACT

Quan, S.; Kvitck, R.; Smith, D., and Griggs, G. 2013, Using vessel-based LIDAR to quantify coastal erosion during El Niño and inter-El Niño periods in Monterey Bay, California. *Journal of Coastal Research*, 29(3), 555–565. Coconut Creek (Florida), ISSN 0749-0208.

Vessel-based light detection and ranging (LIDAR) was employed to collect coastal topography data and to quantify the rates of erosion and spatial distribution of coastal retreat around Monterey Bay, California during the 2008–09 (non-El Niño) and 2009–10 El Niño. These data were compared with pre/post-El Niño LIDAR data from 1997–98 to assess shoreline change and to test the following hypotheses: (1) that broad-scale (km) spatial distribution of erosion rates is positively correlated with wave energy, and (2) that fine-scale erosion hot spots (segments of the coastline exhibiting considerably higher rates of erosion than adjacent areas) shift at predictable alongshore wavelengths between consecutive El Niño and inter-El Niño periods. Broad-scale erosion was found to be significantly higher during the 2009–10 El Niño *vs.* the 2008–09 non-El Niño period in both the south (1.8 m *vs.* 0.1 m average) and north bays (0.5 m *vs.* 0.0 m average). The broad-scale distribution of erosion rates during the 2009–10 El Niño was positively correlated with wave energy. In southern Monterey Bay, erosion rates increased along a wave energy gradient from south to north, whereas erosion and wave energy were both focused and highest at a single location in the northern bay. Fine-scale erosion hot spots were found to occur during the 1997–98 and 2009–10 El Niño and the 1998–08 inter-El Niño period. These hot spots were found to be significantly correlated at –160 m during the 1997–98 El Niño to 1998–2009 inter-El Niño periods and 100 m during the 1998–2009 inter-El Niño to 2009–10 El Niño periods in southern Monterey Bay. Hot spots that occurred during one El Niño or inter-El Niño period shifted spatially alongshore during the subsequent El Niño or inter-El Niño period. Vessel-based LIDAR proved to be effective for detecting coastal change at high spatial resolutions and revealing fine-scale patterns of shoreline retreat.

ADDITIONAL INDEX WORDS: *Shoreline change, erosion rates, seacliff retreat, bluff retreat, coastal geomorphology, remote sensing, coastal processes, El Niño, LIDAR.*

INTRODUCTION

Holocene sea-level rise has produced coastal retreat on a global scale. Erosion is expected to worsen with global warming-induced climate change and accelerated sea-level rise (Church and White, 2006; Varekamp, Thomas, and Van de Plassche, 1992; Zhang, Douglas, and Leatherman, 2004) and an increased intensity of storm events predicted for the 21st century (Meehl *et al.*, 2007).

The primary forcing parameters for coastal erosion along the U.S. west coast (elevated sea levels, increased wave height, and higher precipitation) are associated with moderate to high intensity El Niño Southern Oscillation (ENSO) events (Allan

and Komar, 2006; Storlazzi and Griggs, 2000). Recent documentation of wave height increases along the west coast suggests that one effect of global climate change may be high intensity storms, similar to those experienced during significant ENSO events (Ruggiero, Komar, and Allan, 2010; Seymour, 2011; Storlazzi and Wingfield, 2005). These ENSO events may therefore serve as proxies for anticipated 21st century weather patterns and an opportunity to explore the potential effects of sea-level rise and high intensity storms on shoreline erosion. With an estimated \$184 million in losses, including the destruction of 33 ocean front houses and damage to 3900 homes and business along the U.S. west coast during the 1982–83 El Niño period (Griggs and Johnson, 1983; Griggs and Patsch, 2005), new monitoring and forecasting tools to aid in proactive coastal management are needed to minimize societal impacts of impending climate change.

The ability to more accurately predict where, and at what rates, coastal erosion is likely to occur will be important to

DOI: 10.2112/JCOASTRES-D-12-00005.1 received 7 January 2012; accepted in revision 25 June 2012; corrected proofs received 28 November 2012.

Published Pre-print online 18 December 2012.

© Coastal Education & Research Foundation 2013



www.JCRonline.org

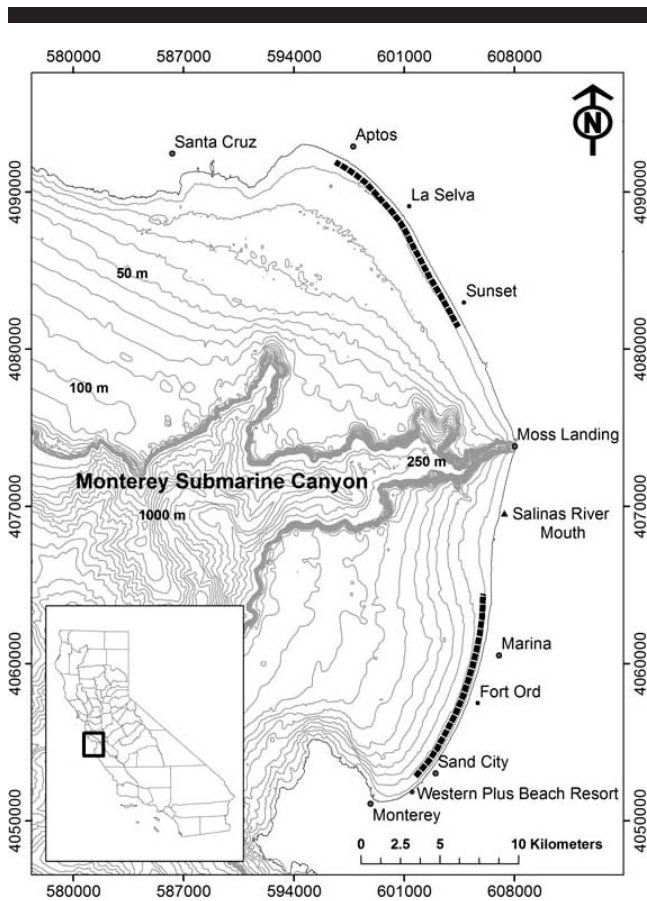


Figure 1. Central California map showing the Monterey Bay coastline and geographical location of the north and south analysis regions (represented with bold dashed lines). Bathymetry contours (10 m) are represented in grey. Coordinate system: UTM zone 10N NAD83.

these planning efforts. Here we use vessel-based mobile topographic light detection and ranging (LIDAR) for shoreline mapping in Monterey Bay, California (Figure 1) to test for predictable differences in spatial and temporal patterns of coastal erosion occurring at different scales during El Niño and inter-El Niño periods.

Monterey Bay

The arcuate shoreline of Monterey Bay along the central California coastline (Figure 1) presents a location uniquely suited to studying spatial variations in coastal retreat. The hooked shape of the headlands at both ends of the bay is in an equilibrium configuration controlled by the interaction of geology and a dominant wave approach from the NW (Griggs and Jones, 1985). This interplay creates large gradients in wave exposure, with the central bay shoreline fully exposed and the north and south extremes partially shielded by their headlands under certain wave conditions. Additionally, the head of Monterey Submarine Canyon in the center of the bay refracts and focuses wave energy to the north and south shores on either side of Moss Landing (Thornton, MacMahan, and

Sallenger, 2007). These steep spatial gradients in wave exposure make the bay an ideal laboratory for testing hypotheses on the relationship between wave energy and patterns of coastal erosion.

Monterey Bay is rimmed by wide sandy beaches that are backed by Flandrian dunes (Cooper, 1967) in the southern section and Tertiary sedimentary rock cliffs and weaker bluffs in the northern section. The north and south headlands consist of more resistant marine sedimentary rocks and granodiorite, respectively (Griggs and Patsch, 2005; Wagner, Greene, and Saucedo, 2002). The strength of the coastal rocks and sediments determines the erodability of the coastline, with softer sediment types having higher susceptibility to erosion *vs.* hard sediment types (Benumof *et al.*, 2000). For this study, sites were restricted to sections of the coastline backed by coastal dunes and bluffs to control for geologic variation in shoreline recession rate analyses (Figure 1).

Long-term erosion (>25 y) rates around Monterey Bay can be traced back to the 1940s and have been found to be persistent and relatively uniform (~0.3–2 m/y) over long time frames (Hapke *et al.*, 2006; Thornton *et al.*, 2006). These studies, based on analysis of historic aerial photographs (Sklavidis and Lima-Blanco, 1985), were focused on broad-scale, long-term assessments of the coastline.

Short-term erosion (<25 y), however, does not occur uniformly in space or time around Monterey Bay but rather in spatially variable “hot spots”; segments of the coastline exhibiting considerably higher rates of erosion than adjacent areas and occur alongshore at scales of 100s of m. This small-scale erosion pattern has been well documented for the 1997–98 El Niño period, with the most extreme rates located in the exposed central section of the bay and decreasing in magnitude toward the more protected southern and northern ends (Egley, 2002; Hapke and Richmond, 2002; Moore and Griggs, 2002; Thornton *et al.*, 2006; Thornton, MacMahan, and Sallenger, 2007). Bluff erosion during the 1997–98 El Niño winter (Oct 1997–April 1998) ranged from 0 to 4 m at Monterey. Rates at Sand City ranged from 0 to 2 m and at Fort Ord from 0.5 to 13 m with net volume loss calculated to be nearly seven times the historic annual average (Thornton *et al.*, 2006).

Direct links were found between hot spot erosion and the formation and location of rip channels and large megacusps (Thornton, MacMahan, and Sallenger, 2007), with the relationship hypothesized to be attributable to narrowing of beach width at mega-cusp embayments, allowing wave run-up to easily reach and erode coastal bluffs (Revell, Komar, and Sallenger, 2002; Shih and Komar, 1994; Thornton, MacMahan, and Sallenger, 2007). The location and formation of rip channels, mega-cusps, and hot spots are hypothesized to migrate and regenerate along the coastline but are not expected to return to their same location the following year because southern Monterey Bay exhibits nearly uniform long-term erosion along sections of the coastline subject to uniform wave exposure (Thornton, MacMahan, and Sallenger, 2007). Given the framework of past studies, we can predict where erosion will occur on long time scales and broad spatial scales, but few researchers have been successful at accurately predicting the location and rate of erosion on short time scales within

local areas due to the spatially variable characteristic of hot spot erosion and the episodic nature of intense storms that appear to control these hot spots (Hapke and Plant, 2010). Considering the impacts to the coastline that occurred during previous El Niño periods, the study and prediction of fine-scale spatial erosion patterns is a crucial step in planning for anticipated increases in shoreline retreat rates.

The quantitative detection of fine-scale hot spot erosion in recent studies was only achievable through the use of high-resolution digital surface models produced from aerial LIDAR data. LIDAR is optical remote sensing using the measurement of time delay between transmittance and return of laser pulses, providing the ability to rapidly and efficiently measure surface geomorphology in three dimensions at high resolution over broad areas. In 1997 and 1998, NASA, USGS, and NOAA collaborated to conduct pre- and post-El Niño airborne LIDAR surveys of the California coastline, providing researchers with digital surface models of the coastline. This data set provided the first clear assessment of El Niño erosion rates in Monterey Bay (Hapke and Reid, 2007; Hapke *et al.*, 2006; Thornton *et al.*, 2006; Thornton, MacMahan, and Sallenger, 2007). Prior to this study there had been only one additional airborne LIDAR survey, which was completed in 2004 by NOAA and USGS, leaving the measurement of erosion rates to be derived by less precise means. While airborne LIDAR has been an effective and groundbreaking method for collecting topographic data by providing high resolution, precision, and broad coverage, the technique has its limitations. Availability, cost, the ability to respond on short notice to significant environmental events, and atmospheric conditions (*e.g.*, low cloud ceilings) that either preclude the use of aircraft or effectiveness of the sensor can limit the use of airborne LIDAR.

Our study employed a vessel-based LIDAR system as an alternative to airborne LIDAR to collect topographic data. This approach combines the high resolution characteristics of LIDAR data with an efficient and effective platform for collecting topographic data. Our expectations were that the high resolution datasets produced using this system would provide insight into the short-term and fine-scale patterns of change that have occurred since the 1998 LIDAR survey and the impacts of the most recent 2009–10 El Niño winter, relative to the 2008–09 normal (non-El Niño) winter, as well as providing a basis for comparing patterns of erosion from two different El Niño periods (1997–98 *vs.* 2009–10).

The project had four objectives: (1) to evaluate the utility of a vessel-based topographic LIDAR system as a rapid-response alternative to airborne LIDAR for collecting coastal topography data and quantifying the spatial distribution of coastal retreat; (2) to use the vessel-based system to quantify and compare the rates and spatial distribution of coastal erosion during the 2008–09 normal (non-El Niño) year and 2009–10 El Niño year and to compare these findings with the results from pre- and post-El Niño airborne LIDAR surveys in 1997 and 1998 (Egley, 2002); (3) to test the assumption that broad-scale erosion is correlated with the spatial distribution of the highest wave energy; and (4) to test the hypothesis that the spatial locations of fine-scale erosion hot spots shift at predictable

alongshore wavelengths between consecutive El Niño and inter-El Niño periods.

METHODS

Vessel-Based LIDAR

We used a Riegl LMS-Z420i terrestrial laser scanner mounted atop a hydrographic survey vessel with its sensor positioned shoreline-normal to produce high resolution topographic datasets at a relatively low cost compared to conventional airborne LIDAR. The Riegl LMS-Z420i (hereafter 420i), originally designed for use as a stationary terrestrial laser scanner, was mounted on the 10 m research vessel *R.V. VenTresca*. The 420i has a range of 1 km, a positional accuracy of 10 mm, and a scan swath angle of 135°. While the 420i was designed to rotate through 360°, in our mobile application the scanner head is fixed in one position and set to line scan mode. This allows for adjacent measurement of coastal relief while the vessel travels parallel to the coast. The scan and acquisition rates for the 420i in a fixed line-scan position are 20 Hz and 8000 points per second, respectively.

Vessel trajectory data were collected to correct the 420i data for platform position and attitude during postprocessing. An Applanix POS/MV 320 was used to collect sensor position and attitude data at 200 Hz. These data were then postprocessed and corrected in Applanix POSpac software with global positioning system (GPS) ephemeris from a network of continuously operating GPS reference stations to yield a tightly coupled inertial-GPS Smoothed Best Estimated Trajectory (SBET) of the 420i's position and attitude (pitch, roll, yaw) referenced to the NAD83 (CORS96 epoch 2002) UTM coordinate system and NAVD88 (Geoid 2003) datum.

The accuracy and precision of this coupled mobile system (Riegl LMS-Z420i and Applanix POS/MV 320) was quantified by scanning six separate target locations on different dates both before and after the shoreline surveys at which a Trimble NetR5 GPS receiver was set up collecting static L1/L2 GPS fixes. The static GPS data were postprocessed using the National Geodetic Survey Online Positioning User Service (OPUS). All six targets were scanned at ranges between 50 and 100 m. The LIDAR-derived solutions for repeat scans of each target varied by <0.04 m horizontally and vertically, and the mean horizontal and vertical LIDAR solutions for each target were all within 0.10 m of the corresponding static GPS solutions.

Vessel-based LIDAR data were collected along the shoreline of Monterey Bay on December 9 and 10, 2008; November 4, 2009; and on July 15, 16, and 17, 2010, during low tide and relatively calm seas (Figure 1). These conditions are optimal for vessel-based LIDAR measurements as collection during low tide provides the fullest coverage of the shoreline relief. Rough seas increase boat motion and can therefore reduce data density as the laser sensor's swath covers relatively more sky and water and less shoreline when rolling heavily.

The raw vessel-based LIDAR data contained time, range, bearing, and intensity information all relative to the scanner's geometrical center. Riegl RiScanPro software was used to apply SBET solutions to the raw LIDAR data, yielding correctly georeferenced XYZ data in NAD83 (CORS96 epoch 2002) UTM

coordinate system and NAVD88 (Geoid 2003) vertical datum. The XYZ data densities were generally five points per m².

Postsurvey ground-truthing was completed to verify the accuracy and precision of these georeferenced vessel-based LIDAR datasets. The positions of three clearly identifiable objects visible in the LIDAR point clouds from three sections of the Monterey Bay coastline (south, central, and north) were independently measured with a Trimble NetR5 GPS receiver and postprocessed in OPUS. The postprocessed static GPS positions were then compared on a point-by-point basis to those of their respective targets visible in all three vessel-based LIDAR survey datasets.

Fledermaus (IVS3D) software was used for editing and 3D visualization of vessel-based LIDAR data. This process involved the manual rejection of outliers on a point-by-point basis based on visual interpretation of the colinearity between points. Digital elevation models (DEM) in ArcGrid format were generated in Fledermaus at 1 m resolution using the mean squares algorithm. These DEMs were subsequently used in ArcGIS (ESRI) for analysis.

Pre-existing data from the collaborative USGS, NASA, and NOAA airborne LIDAR surveys conducted on October 12 and 13, 1997, and April 15, 17, and 18, 1998, via NASA's Airborne Topographic Mapper (ATM) were also used in conjunction with the vessel-based LIDAR from this study for shoreline change analyses. These earlier LIDAR data sets were downloaded as georeferenced XYZ point cloud data and processed using the same editing and gridding techniques used with the 420i data, but with an output resolution of 2 m because of their lower point densities. Unfortunately, the 2004 NOAA and USGS LIDAR results could not be included in this analysis because of coverage gaps in those data for the north and south bay study areas used here.

GIS Analyses

Previous researchers have employed a variety of geomorphic reference features to measure shoreline recession including the intersection of the back beach and dune apron (Thornton *et al.*, 2006), top of the seacliff face (Hapke and Reid, 2007; Hapke, Reid, and Richmond, 2009) and the "high tide line" (Hapke *et al.*, 2006). Each of these approaches has its advantages and limitations, and the decision of which method and reference feature to use may depend on the type of data available, the nature of the coastal topography, accessibility of the site, or personal preference. The intersection of the back beach and dune can oscillate back and forth seasonally, so it may not be an optimal feature to monitor depending on the time scale of the study. The seacliff top captures bedrock erosion but can be difficult to delineate in DEMs where the break in slope or change in aspect is not as pronounced for some gently sloping coastal bluffs. Because "bedrock" represents the local geologic material that best resists erosion, its landward retreat can be used as the basis for monitoring long-term coastal erosion. In the Monterey Bay study area, bedrock locally includes weak marine sandstone, poorly lithified Quaternary dunes, and modern dunes, all of which are subject to relatively rapid erosion.

The use of high density LIDAR data provides significant flexibility in selecting the geomorphic feature to monitor. For

this study our chief criteria in selecting a reference feature included the following factors. (1) It must be the most resistant material present in order to capture monotonic, parallel retreat of the eroding coastline; (2) it must foster reproducibility for future vessel-based and airborne LIDAR studies; and (3) it must have a high density of LIDAR strikes to ensure high precision.

For the purposes of this study we chose to measure coastal position and change on the seacliff face along the 10-meter elevation contour (NAVD88). This reference contour was selected based on field inspections throughout the study area that revealed this elevation to be the one most representative of the local bedrock face because it was generally well above the seacliff sand apron but below the often low seacliff tops (Figure 2).

The Digital Shoreline Analysis System (DSAS; Thielier *et al.*, 2009) was used to calculate shoreline recession along the coastline at the 10 m contour (NAVD88) derived in ArcGIS for each dataset. Transects were spaced at 20 m intervals and oriented normal to the coastline to accommodate any crenulated cliffs and to facilitate comparison with previous USGS (Hapke and Reid, 2007; Hapke *et al.*, 2006; Morton and Miller, 2005) and DSAS (Hapke, Reid, and Richmond, 2009) cliff-change analyses. The analysis was broken up into southern and northern Monterey Bay sections approximately 10 km and 11 km in length, respectively (Figure 1). Net erosion based on reference feature movement was calculated for each transect using the horizontal shift in the 10 m contour line position. In order to achieve the most accurate measure of net shoreline change at the location of each transect, the otherwise shoreline-normal orientation of individual transects was edited to be normal to the seacliff face in deeply crenulated cliffs according to the methods of Hapke *et al.* (2006). One Way Analysis of Variance (ANOVA) and Welch's Two Sample *t*-test were used to test for significant differences between the 1997–98 El Niño, 1998–2009 inter- El Niño, 2008–09 non- El Niño, and 2009–10 El Niño periods for southern Monterey Bay and northern Monterey Bay, respectively.

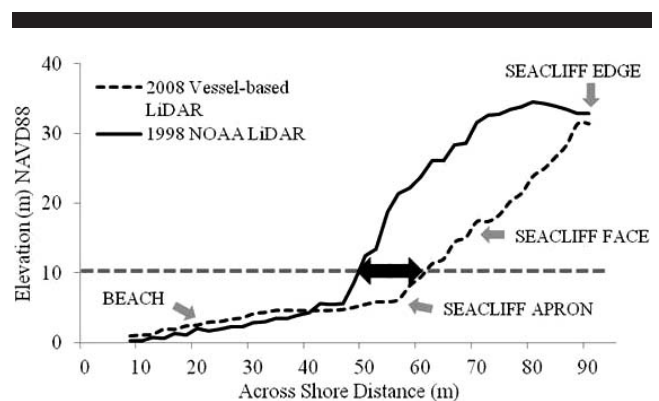


Figure 2. Shore-normal profiles of 1998 and 2008 LIDAR digital elevation models showing an example of shoreline recession measurement with the erosion reference feature being the position of the seacliff face at 10 m elevation NAVD88 (grey dashed line).

Total positional uncertainty for the net shoreline movement calculations were derived using methods from Hapke *et al.* (2006) and Stockdon *et al.* (2002). Net erosion reference feature movement uncertainty was calculated as the quadrature summation of LIDAR data uncertainty and contour derivation uncertainty. The independently measured GPS positions of three objects along the Monterey Bay coastline initially used for ground-truthing were compared with their respective positions in the vessel-based LIDAR point clouds. The root mean square (RMS) was calculated for each x , y , and z for each dataset (RMS_x , RMS_y , and RMS_z), comparing the position of coastal structures in all vessel-based LIDAR datasets to their respective static GPS positions. The root sum of squares (RSS) or combined RMS for each x , y , and z position was used for an estimate of vessel-based LIDAR uncertainty. Due to the lower data densities of the 1997 and 1998 LIDAR, point-to-point comparisons with independently measured GPS positions were not possible. Therefore, airborne LIDAR uncertainty estimate was derived from existing airborne LIDAR studies on NASA's ATM (Sallenger *et al.*, 2003) at 0.15 m.

Contour derivation uncertainty was estimated by extracting horizontal positions in all datasets at a structurally sound vertical feature at a fixed vertical elevation. We used the Best Western Plus Beach Resort Monterey seawall for that purpose (Figures 1 and 3). Contours from each data set were generated across the sea wall at 5 m elevation (NAVD 88). Two shore-normal transects were generated randomly along the seawall and were used to intersect the generated contours to extract horizontal positions at each intersection. RMS was calculated for each UTM easting (RMS_x) and (RMS_y), comparing the mean x and y positions. RSS for both RMS_x and RMS_y were used as an estimate for contour derivation uncertainty.

Running averages were conducted on the results of the DSAS net shoreline movement analysis to minimize noise and reveal the spatial periodicity of erosion hot spots. A shoreline segment length of 100 m for the running average was used to give a clear signal because that value is less than the spatial scales of the estimated 200–300 m mega-cusp-length hot spots located in Monterey Bay (Thornton, MacMahan, and Sallenger, 2007).

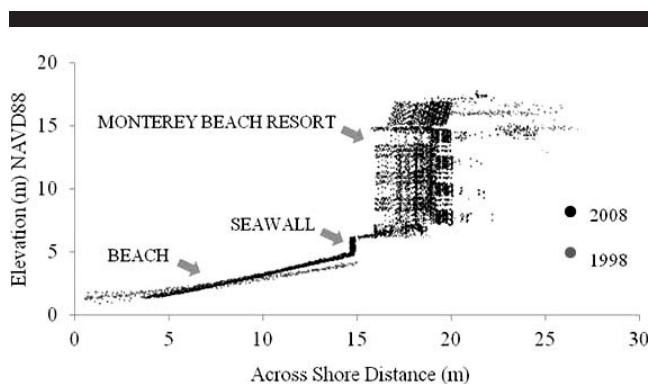


Figure 3. Shore-normal profiles of 2008 vessel-based LIDAR and 1998 aerial LIDAR to assess intersurvey precision. Location: Monterey Bay Beach Resort.

Cross-correlation analysis was used to test the hypothesis that erosion hot spots exhibit a predictable alternating spatial pattern alongshore between consecutive El Niño and inter-El Niño periods. Digital Shoreline Analysis System results for consecutive El Niño and inter-El Niño periods from 1997–2010 were cross-correlated in sequence (1997–98 El Niño then 1998–2009 inter- El Niño, 1998–2009 inter-El Niño then 2009–2010 El Niño) to identify the displacement of maximum correlation or the mean shift between hot spot shorelines relative to each other.

Coastal Data Information Program (CDIP) swell-height distribution NOWcast models (250 m resolution) were used to generate a mean composite for the 2009–10 El Niño period to compare swell-height distribution with seacliff erosion rate values in Monterey Bay. The five strongest El Niño storms were selected using a compilation of National Buoy Data Center significant wave height and tidal height data. The greatest combination of high significant wave height and high tidal height at any given period was used to determine the five strongest El Niño winter storms (October 15, 2009; November 28, 2009; January 19, 2010; February 13, 2010; and February 28, 2010). Coastal Data Information Program swell-height distribution NOWcast models for each of the five selected El Niño winter storms were downloaded as 8-bit bitmap images, reclassified, and merged in ArcGIS to create a mean composite of wave height distribution of the five strongest storms for the 2009–10 El Niño year at 250 m spatial resolution. Digital Shoreline Analysis System results were binned to closely match the 250 m resolution of the mean composite swell-height distribution model and statistically compared with regression analyses.

RESULTS

Ground truth surveys of three coastal structures along the Monterey Bay coastline compared to all of the vessel-based LIDAR datasets yielded differences ranging from -0.36 to 0.20 m in easting, from -0.04 to 0.17 m in northing, and from -0.11 to 0.14 m vertically. Total vessel-based LIDAR RMS_x , RMS_y , and RMS_z were 0.25 m, 0.28 m, and 0.16 m, respectively. The RSS of RMS_x , RMS_y , and RMS_z for vessel-based LIDAR was 0.41 m. Because of the point-to-point comparisons, error may be attributable to sparse data density particularly at the coastal structures that were independently surveyed. Other sources of error include LIDAR system accuracy, which Riegler estimates is 0.10 m.

Easting and northing position comparisons of the 1998, 2008, 2009, and 2010 LIDAR datasets at the Best Western Plus Beach Resort Monterey seawall at 5 m (NAVD88) yielded differences ranging from -1.0 to 0.7 m easting and from -0.7 to 0.1 m northing. Unfortunately, the 1997 data set did not cover the seawall site. Total RMS_x and RMS_y were 0.9 m and 0.9 m, respectively. The RSS of RMS_x and RMS_y was 1.3 m. The total positional uncertainty, composed of the RSS of vessel-based LIDAR, airborne LIDAR, and contour derivation uncertainty, was 1.4 m, which is consistent with previous LIDAR positional uncertainty estimates (Stockdon *et al.*, 2002). Sources of error are attributable to grid generation using the mean squares algorithm and the generation of contour lines from these grids.

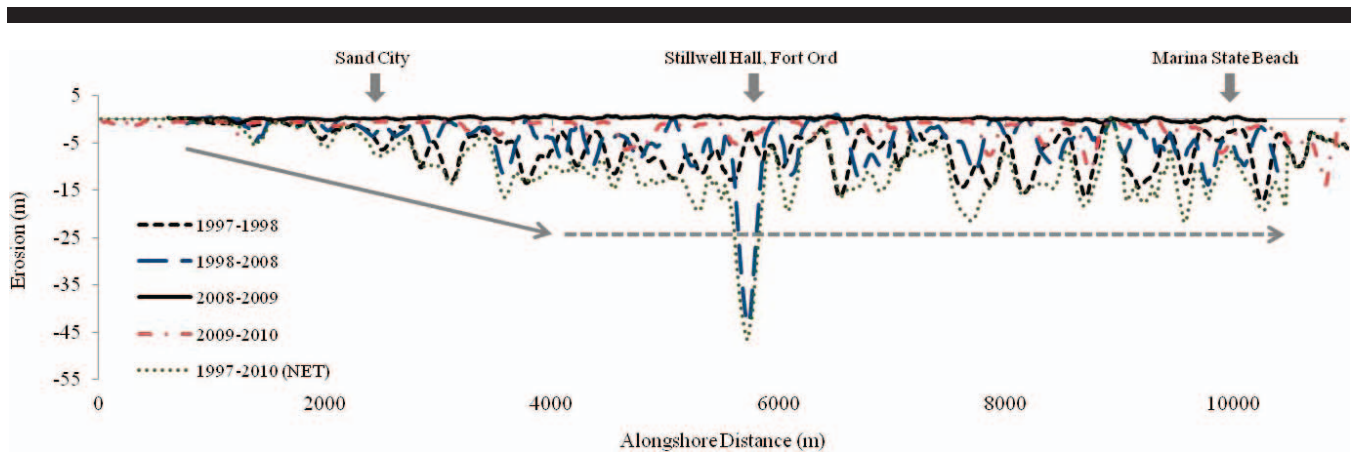


Figure 4. Southern study area plot of shoreline recession with a 100 m running average at 10 m elevation (NAVD88). X axis represents alongshore distance (m) starting in Sand City and ending at Marina Sate Beach. Y axis represents shoreline recession (m). The solid line depicts a trend of increasing erosion magnitude alongshore, whereas the dashed line depicts signs of shoreline averaging found along this stretch of coastline.

Erosion results for this study are reported raw (*i.e.*, without account for uncertainty estimates) and on a per period basis (*i.e.*, survey date to survey date). Annualizing these rates can yield misleading results because coastal erosion is highly seasonal along the U.S. west coast, with most erosion occurring in winter months. In keeping with previous work, results show numerous spatially variable erosion hot spots that increase in occurrence and magnitude along a gradient from south to north

along southern Monterey Bay during the 2009–10 El Niño period (Figure 4). Although moderate in severity compared to the 1997–98 El Niño period, substantial erosion occurred during the 2009–10 El Niño. The highest rates of shoreline recession were detected between Fort Ord Dunes State Beach at the old Stillwell hall site (~14 m) and at Marina Beach (~8 m) during the 2009–10 El Niño (Figures 4 and 5) with an average of 1.8 m (Table 1). Although erosion during the 2008–09 non-El Niño period was minor and fell below our estimated level of uncertainty, considerably higher rates of erosion were found during the 2009–10 El Niño period (1.8 m average) than the 2008–09 non-El Niño period (0.1 m average) (Table 1). Significant differences were found between erosion during the 1997–98 El Niño, 1998–2009 inter- El Niño, 2008–09 non- El Niño, and 2009–10 El Niño periods for southern Monterey Bay (Table 1).

Spatially variable erosion hot spots were also detected in southern Monterey Bay during the inter-El Niño period (1998–2009) with an erosion average of 3.7 m (Table 1). Multi-El Niño cycle (1997–2010) analyses revealed a stronger south to north gradient signal, which was only slightly apparent in the 2009–10 El Niño for the same region (Figure 4). During the multi-El



Figure 5. Aerial photographs of the Marina launch ramp at Marina State Beach captured in 2008 and 2010. Shoreline recession was measured at up to 8 m in this area. [Photos copyright (c) 2010, Adelman and Adelman (2010), Kenneth and Gabrielle Adelman, California Coastal Records Project, www.californiacoastline.org.] Resistant horizontal band in sealiff is a paleosol within the Quaternary Aromas Red Sandstone depicted with the horizontal black arrows.

Table 1. Summary of average shoreline change rates for Monterey Bay derived from DSAS results. Asterisks denote p values (0.01*, 0.001**, <0.001***) for ANOVA (Southern Monterey Bay 1997–98, 1998–2009, 2008–2009, and 2009–2010 periods) and Welch Two Sample t-test (Northern Monterey Bay 2008–09 and 2009–10 periods) tests.

	Average Erosion (m)	±95% Ci (m)	SD (m)	N
Southern Monterey Bay				
2009–10 El Niño period	-1.8***	0.15	1.7	484
2008–09 Inter-El Niño year	-0.1***	0.03	0.3	484
1998–2009 Inter-El Niño period	-3.7***	0.30	3.4	484
1997–98 El Niño period	-6.4***	0.37	4.1	484
Northern Monterey Bay				
2009–10 El Niño period	-0.5***	0.04	0.44	408
2008–09 Inter-El Niño year	-0.0***	0.01	0.14	408

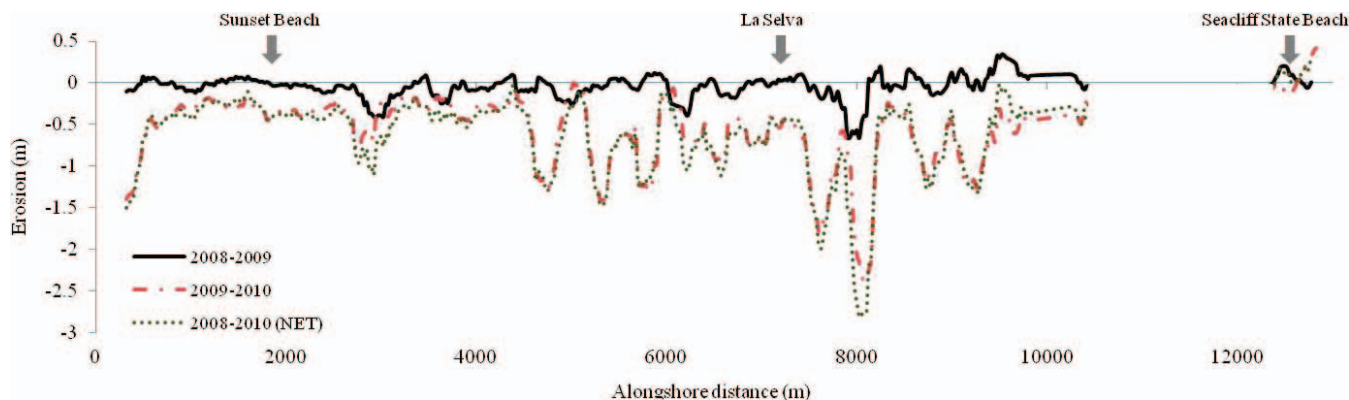


Figure 6. Northern study area plot of shoreline recession with a 100 m running average at 10 m elevation (NAVD88). X axis represents alongshore distance (m) starting from Sunset Beach and ending at Seacliff State Beach. Y axis represents shoreline recession (m).

Niño cycle (1997–2010), erosion magnitude increased at an approximate rate of 5 m of retreat per km alongshore for the first 0 to 4 km of coastline starting 2 km SW of Sand City (Figure 4). The 8 km of coastline between Sand City and Marina exhibited signs of shoreline averaging, where erosion is persistent and relatively uniform over long timeframes, as there were no obvious alongshore trends in erosion magnitude over large spatial and temporal scales.

In northern Monterey Bay, erosion during the 2009–10 El Niño period was minimal compared to the southern bay, with an overall mean of 0.5 m (Table 1). Erosion reached a maximum of 2.5 m at erosion hot spots near La Selva (Figure 6). Mean erosion during the 2008–09 normal year was 0.0 m for northern Monterey Bay (Table 1). Significant differences were also found between erosion during the 2008–09 non-El Niño and 2009–10 El Niño periods for northern Monterey Bay (Table 1), but the overall results fall below our level of estimated total positional uncertainty.

A comparison of the spatial locations of El Niño and inter-El Niño hot spots in southern Monterey suggests the occurrence of a hot spot migration process during consecutive 1997–98 El Niño to 1998–2009 inter-El Niño periods and 1998–2009 inter-El Niño to 2009–10 El Niño periods (Figure 7). For the majority of the coastline, hot spots that occurred during one period tend to have little or no activity in the consecutive period.

Cross correlations of El Niño and inter-El Niño erosion hot spot variations were found to be significantly correlated at 95% confidence at –160 m during the 1997–98 El Niño to 1998–2009 inter-El Niño periods and 100 m during the 1998–2009 inter-El Niño to 2009–10 El Niño periods in southern Monterey Bay (Figure 8). Erosion hot spots that occurred during one El Niño or inter-El Niño period shifted spatially alongshore during subsequent El Niño or inter-El Niño period.

The composite swell-height distribution model for the 2009–10 El Niño period revealed gradients and variations of wave height in Monterey Bay (Figure 9). In northern Monterey Bay high wave energy was found at La Selva Beach with the remainder of the northern coastline, exhibiting relatively uniform wave-energy exposure. In southern Monterey Bay a

strong gradient of increasing swell height from south to north was found centered on Sand City. The shoreline adjacent to this gradient from north of Sand City to the Salinas river mouth is characterized by uniform wave-energy exposure. The highest wave energy occurred at the muted delta of the Salinas River, indicated by seaward deflected isobaths near the Salinas River mouth (Figure 1). As expected, results from both El Niño and inter-El Niño analyses indicate that locations with the highest rates of erosion coincided with the locations of highest wave energy. In the southern Monterey Sand City region the wave-energy gradient coincided with the erosion gradient, and in northern Monterey Bay the area of highest wave energy coincided with the erosion hot spot at La Selva (Figures 4, 6, and 9).

The DSAS results are plotted with wave height data for both southern and northern Monterey Bay (Figure 10). Wave height values were selected at 100 m offshore relative to the shoreline to omit erroneous breaking wave zone data. Exponential (southern Monterey Bay) and linear (northern Monterey Bay) regression results indicate significant relationships between shoreline recession and wave height ($p < 0.05$, northern Monterey Bay adjusted $R^2 = 0.1621$).

DISCUSSION

Consistent with previous pre/post-El Niño shoreline assessments (Hapke and Richmond, 2002; Moore and Griggs, 2002; Thornton *et al.*, 2006), spatially variable erosion hot spots occurred during the 2009–10 El Niño period and at significantly higher rates of change than during the 2008–09 normal year. The southern Monterey Bay coastline changed considerably from 1997 to 2010, with both El Niño and inter-El Niño periods playing important roles in coastal erosion. Erosion during the two El Niño periods (1997–98, 2009–10) produced the greatest change over short time frames, but erosion during the 11-year inter-El Niño period (1998–2009) contributed to substantial net change at a lower rate. Hot spot erosion was previously found to occur only during El Niño or extreme storm events (Thornton *et al.*, 2006, Thornton, MacMahan, and Sallenger, 2007), but in

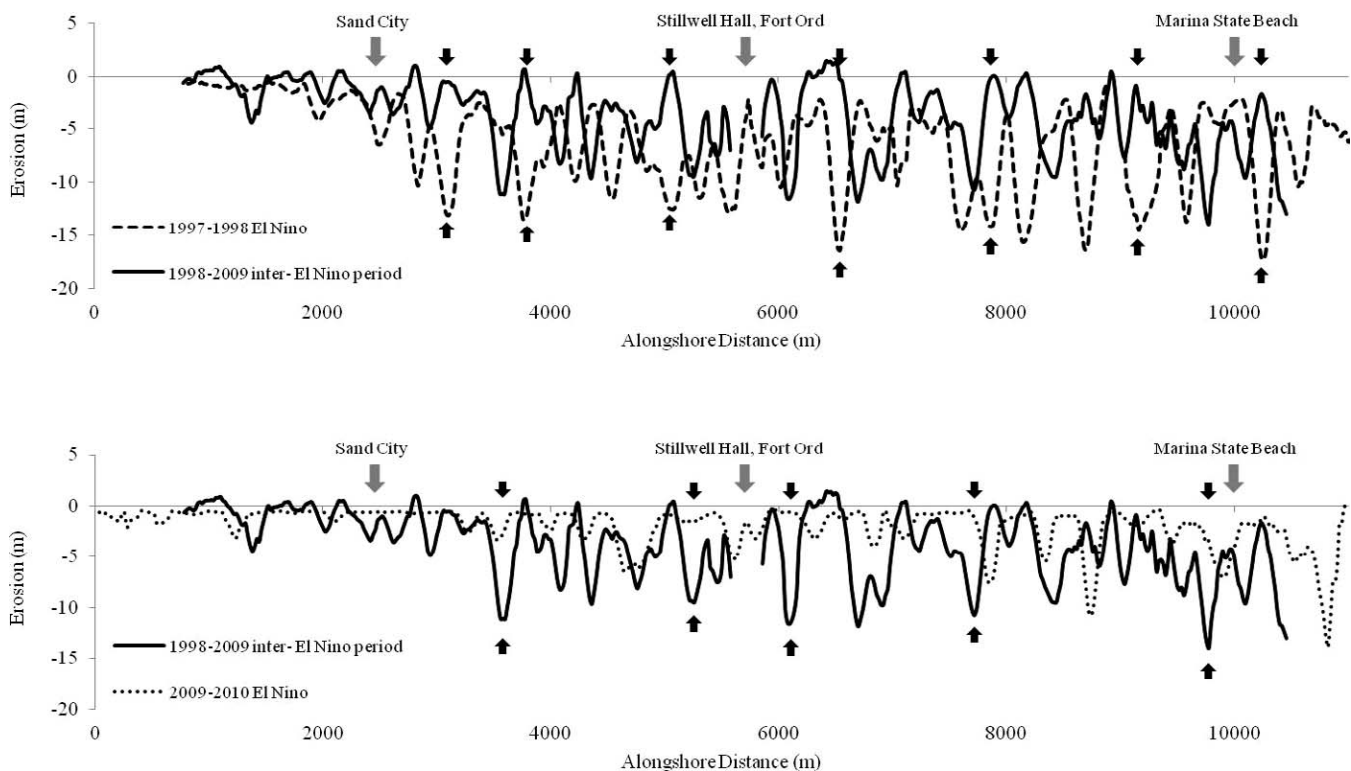


Figure 7. Plots of shoreline recession after consecutive El Niño to inter-El Niño periods (top) and inter-El Niño to El Niño periods (bottom) with a 100 m running average at 10 m elevation (NAVD88) for Southern Monterey Bay. X axis represents alongshore distance (m) starting in Sand City and ending at Marina Sate Beach. Y axis represents shoreline recession (m). Black arrows indicate some erosion hot spot shift locations. Anomalously high shoreline recession values at Stillwell hall were omitted.

this study hot spot erosion was shown to occur during both El Niño and inter-El Niño periods.

Net alongshore erosion at the decadal time scale spanning two El Niños and the inter-El Niño period from 1997 to 2010 in southern Monterey Bay was found to exhibit signs of shoreline averaging over the 8 km of shoreline north of the identified wave energy gradient at Sand City (Figure 4). One anomaly in this trend of uniform long-term retreat occurred at Stillwell Hall in Fort Ord. Coastal armoring at that site created a local promontory, relative to the adjacent coastline. When a riprap seawall was removed from the bluff toe in 2004, the promontory quickly retreated with respect to the adjacent unmodified seacliffs (Figures 4 and 11). Analysis of swell-height distribution with results from the DSAS yielded significant correlation between swell height and shoreline recession (Figure 10). Along the southern bay shoreline, where the sandy bluffs are uniformly weak and susceptible to erosion, wave distribution models may prove to be a reliable predictor for future coastal erosion on broad scales in this region.

The alongshore shifts in the locations of erosion hot spots that were found in southern Monterey Bay when comparing consecutive El Niño and inter-El Niño periods (1997–98 El Niño to 1998–2009 inter-El Niño to 2009–10 El Niño) (Figure 7) suggest the occurrence of a hot spot migration or jump process

in which the spatial location of erosion hot spots shift north or south between consecutive El Niño and inter-El Niño periods.

Cross correlations of El Niño and inter-El Niño erosion hot spot variations indicated an average hot spot shift of 160 m to the south between the 1997–98 El Niño relative to 1998–2009 inter-El Niño periods and an average hot spot shift 100 m to the north between the 1998–2009 inter-El Niño relative to 2009–10 El Niño periods in southern Monterey Bay (Figure 8). These results also indicate a net shift of 60 m south between the 1997–98 and 2009–10 El Niños. The relevant length scale (distance between peak maxima) from the two cross correlation analyses are 320 m for the 1997–98 El Niño to 1998–2009 inter-El Niño period and 200 m for the 1998–2009 inter-El Niño to 2009–10 El Niño period. These values match up well with the mean spacing of hot spots found in the DSAS results and the estimated 200–300 m mega-cusp lengths alongshore (Thornton, MacMahan, and Sallenger, 2007).

Previous work has shown that rip currents migrate with mega-cusps, and that the formation and location of mega-cusps play a significant role in the amount of wave run-up and subsequently the potential for erosion hot spots (Thornton, MacMahan, and Sallenger, 2007). Rip currents were found to migrate throughout the year during both El Niño (Thornton, MacMahan, and Sallenger, 2007) and non-El Niño years (Orzech *et al.*, 2010). Orzech *et al.*, 2010 found rip channels in

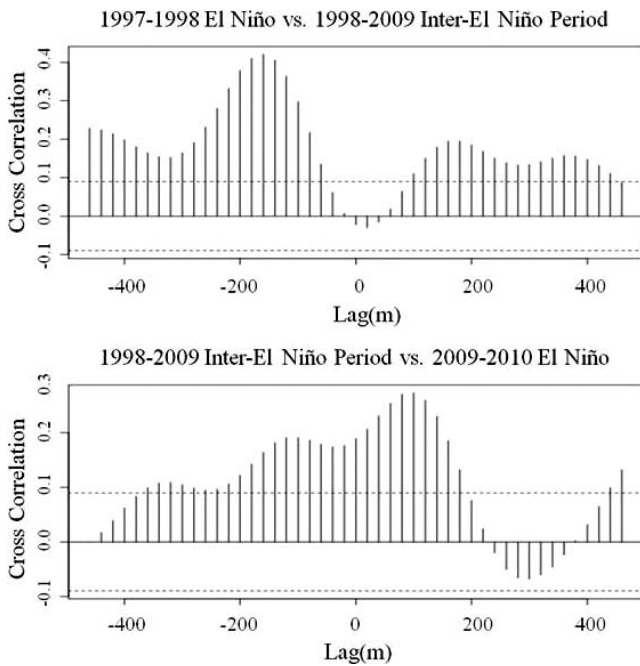


Figure 8. Cross-correlations between consecutive El Niño and inter-El Niño period hot spot erosion for Southern Monterey Bay. The most significant cross correlation values were found at a spatial lag of -160 m (top) and 100 m (bottom), indicating mean alongshore shifts in hot spot locations between periods. Horizontal dashed lines represent 95% confidence levels. Anomalously high shoreline recession values at Stillwell Hall were omitted.

the center of southern Monterey Bay to slowly migrate south during most of the year and migrate north at a faster rate during the winter with nearly no net annual migration. A complicated coastal process presents itself as mega-cusps migrate up and down annually along the southern Monterey Bay shoreline, and hot spots occur variably only during times with coincident large waves and high tides. Measurements in this study only serve as snapshots sometime during this complicated process. Therefore, we can only speculate on the processes that cause the shifts in erosion hot spot location (*i.e.*, migration or jump) found in this study.

The detection of hot spot shifts between consecutive El Niño and inter-El Niño periods aids in short-term coastal management decisions for southern Monterey Bay. Previously interpreted as primarily episodic and variable, occurring during extreme storm periods characteristic of El Niño episodes, results from this study along with previous studies (Orzech *et al.*, 2010) demonstrate that relatively rapid erosion can also occur during quiescent periods. These hot spots are not expected to grow in the same location during the following period but will migrate (or jump) so that the mean shoreline averaged over broad scales and long timeframes recesses at the same rate. This process apparently leads to the overall gently curving nature of the shoreline/bluff edge at both ends of the bay (Griggs and Jones, 1985).

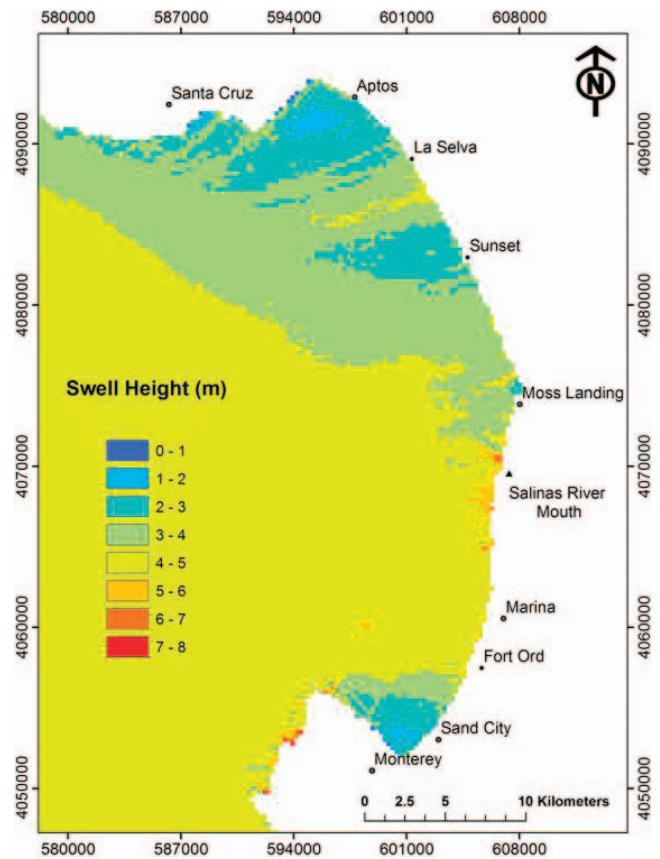


Figure 9. Coastal Data Information Program mean swell height distribution NOWcast model composite (250 m cell size) derived from the five strongest 2009–10 El Niño winter storms (October 15, 2009; November 28, 2009; January 19, 2010; February 13, 2010; and February 28, 2010). Coordinate system: UTM zone 10N NAD83.

Given the complicated fine-scale coastal processes that occur in Monterey Bay, there is great need for new, efficient, and cost-effective tools for precisely monitoring the distribution and rates of coastal erosion over shorter time frames to enable more

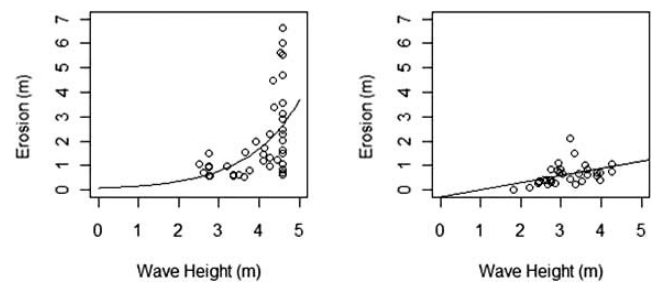


Figure 10. Bluff erosion (m) plotted against average wave height (m) for southern Monterey Bay (left, $N=46$) and northern Monterey Bay (right, $N=34$) during the 2009–10 El Niño period with their respective exponential (left) and linear (right) regression lines.



Figure 11. Aerial photographs of Stillwell Hall at Fort Ord captured in 2002 and 2010. [Photos copyright (c) 2010, Adelman and Adelman (2010), Kenneth and Gabrielle Adelman, California Coastal Records Project, www.californiacoastline.org.] This location is a good example of passive erosion fronting coastal armoring, which can be recovered with armor removal.

nimble adaptive management in response to accelerating climate change and sea-level rise. The flexible, rapidly mobilized vessel-based LIDAR system used in this study produces high resolution terrain data in a relatively cost-effective manner compared to traditional airborne LIDAR surveys, for which high cost is one of the biggest limiting factors for repeat aerial LIDAR surveys. Because of its low, horizontal viewpoint, vessel-based LIDAR, unlike airborne LIDAR, can miss flat spots above the level of the sensor and topographic lows behind berms and dunes. While this limitation precludes the ability to measure back dunes, vessel-based LIDAR is optimal for measuring shoreline recession, deposition, and topography of seacliff faces. This horizontal viewpoint is particularly effective for measuring marine terrace and steep seacliff faces: topographic features that aerial LIDAR's down-looking viewpoint can miss and/or misrepresent because of sparse data density.

CONCLUSIONS

Vessel-based LIDAR data collected in 2008, 2009, and 2010 and pre-existing USGS, NASA, and NOAA airborne topographic LIDAR data from 1997 and 1998 were analyzed using spatial analysis tools in ArcGIS to quantify alongshore erosion during the 1997–98 El Niño, 1998–2009 inter-El Niño period, and 2009–10 El Niño for the Monterey Bay shoreline.

Erosion occurred during the 1997–98 El Niño and 2009–10 El Niño in southern Monterey Bay and was found to be

significantly higher during the 2009–10 El Niño *vs.* the 2008–09 non-El Niño period (1.8 m average *vs.* 0.1 m average in the southern bay and 0.5 m average *vs.* 0.0 m average in the northern bay). Spatially variable hot spots were found post 2009–10 El Niño, and although moderate compared to 1997–98, substantial erosion occurred during the 2009–10 El Niño. El Niño and inter-El Niño erosion hot spot variations were found to be significantly correlated at the 95% confidence at –160 m during the 1997–98 El Niño to 1998–2009 inter-El Niño periods and 100 m during the 1998–2009 inter-El Niño to 2009–10 El Niño periods in southern Monterey Bay. Erosion hot spots that occurred during one El Niño or inter-El Niño period shifted spatially alongshore during the subsequent El Niño or inter-El Niño period. The DSAS shoreline recession results during the multi-El Niño cycle (1997–2010) indicate signs of shoreline averaging over large spatial and temporal scales along the southern Monterey Bay coastline with net erosion consistent with significant wave energy. This correspondence suggests that wave energy distribution models may prove valuable as reliable predictors of future coastal erosion on broad scales.

The utilization of vessel-based LIDAR proved to be an effective and efficient method for the collection of high resolution shoreline topographic data, able to support the accurate and precise quantification, analysis, and modeling of small-scale geomorphic coastal processes. With the effects of global warming and sea-level rise projected to exacerbate coastal erosion, this approach offers a cost-effective alternative for conducting the more frequent seasonal and event-driven repeat surveys required for long- and short-term change analyses.

ACKNOWLEDGMENTS

This study analyzed data collected by the CSUMB Seafloor Mapping Lab for the California Ocean Protection Council's California Seafloor Mapping Project. We gratefully acknowledge the technical assistance of the CSUMB Seafloor Mapping Lab staff, as well as S.W. Moore, C.D. Garza, and D.M. Fernandez. We appreciate the thorough and constructive reviews provided by E.B. Thornton and four anonymous reviewers.

LITERATURE CITED

- Adelman, K. and Adelman, G., 2010. California Coastal Records Project. www.californiacoastline.org.
- Allan, J.C. and Komar, P.D., 2006. Climate controls on US west coast erosion processes. *Journal of Coastal Research*, 22(3), 511–529.
- Benumof, B.T.; Storlazzi, C.D.; Seymour, R.J., and Griggs, G.B., 2000. The relationship between incident wave energy and seacliff erosion rates: San Diego County, California. *Journal of Coastal Research*, 16(4), 1162–1178.
- Church, J.A. and White, N.J., 2006. A 20th century acceleration in global sea level rise. *Geophysical Research Letters*, 33, L01602.
- Cooper, W.S., 1967. Coastal Dunes of California. *Memoir 104 of the Geological Society of America*, 131p.
- Egley, L.A., 2002. An Application of Lidar to Examine Erosion in the Southern Monterey Bay during the 1997–98 El Niño. Monterey, California: Naval Postgraduate School, Master's thesis, 74p.
- Griggs, G.B. and Johnson, R.E., 1983. The impact of 1983 storms on the coastline of northern Monterey Bay. *California Geology*, 36, 163–174.
- Griggs, G.B. and Jones, G.D., 1985. Erosion along an "Equilibrium" Coastline, California's Battered Coast. *Conference Proceedings*,

- California Coastal Commission. San Diego, California, pp. 102–119.
- Griggs, G.B. and Patsch, K., 2005. Año Nuevo to the Monterey Peninsula. In: Griggs, G., Patsch, K., and Savoy, L. (eds.), *Living with the Changing California Coast*. Berkeley: University of California Press, pp. 228–269.
- Hapke, C.J. and Plant, N., 2010. Predicting cliff erosion using a Bayesian probabilistic model. *Marine Geology*, 278, 140–149.
- Hapke, C.J. and Reid, D., 2007. National Assessment of Shoreline Change Part 4. Historical Coastal Cliff Retreat along the California Coast: *United States Geological Survey Open File Report 2007-1133*, 57p.
- Hapke, C.J. and Richmond, B.M., 2002. The impact of climatic and seismic events on the short-term evolution of seacliffs based on 3-D mapping: Northern Monterey, California. *Marine Geology*, 187 (3–4), 259–278.
- Hapke, C.J.; Reid, D., and Richmond, B., 2009. Rates and trends of coastal change in California and the regional behavior of the beach and cliff system. *Journal of Coastal Research*, 25(3), 603–615.
- Hapke, C.J.; Reid, D.; Richmond, B.M.; Ruggiero, P., and List, J., 2006. National Assessment of Shoreline Change Part 3. Historical Shoreline Change and Associated Coastal Land Loss along the Sandy Shorelines of the California Coast: *United States Geological Survey Open File Report 2006-1219*, 79p.
- Meehl, G.A.; Stocker, T.F.; Collins, W.D.; Friedlingstein, P.; Gaye, A.T.; Gregory, J.M.; Kitoh, A.; Knutti, R.; Murphy, J.M.; Noda, A.; Raper, S.C.B.; Watterson, I.G.; Weaver, A.J., and Zhao, Z.C., 2007. Global Climate Projections. In: Solomon, S.; Qin, D.; Manning, M.; Chen, Z.; Marquis, M.; Averyt, K.B.; Tignor, M., and Miller, H.L. (eds.), *Climate Change 2007: The Physical Science Basis. Contribution of Working Group I to the Fourth Assessment Report of the Intergovernmental Panel on Climate Change*. Cambridge University Press: Cambridge, United Kingdom and New York, USA.
- Moore, L.J. and Griggs, G.B., 2002. Long-term cliff retreat and erosion hot spots along the central shores of the Monterey Bay National Marine Sanctuary. *Marine Geology*, 181, 265–283.
- Morton, R.A. and Miller, T.L., 2005. National Assessment of Shoreline Change, Part 2: Historical Shoreline Changes and Associated Coastal Land Loss along the U.S. Southeast Atlantic Coast: *U.S. Geological Survey Open File Report 2005-1401*, 40p.
- Orzech, M.D.; Thornton, E.B.; MacMahan, J.H.; O'Reilly, W.C., and Stanton, T.P., 2010. Alongshore rip channel migration and sediment transport. *Marine Geology*, 271, 278–291.
- Revell, D.L.; Komar, P.D., and A.H., Jr., Sallenger, 2002. An application of LIDAR to analyses of El Niño erosion in the Netarts Littoral Cell, Oregon. *Journal of Coastal Research*, 18(4), 792–801.
- Ruggiero, P.; Komar, P.D., and Allan, J.C., 2010. Increasing wave heights and extreme value projections: the wave climate of the U.S. Pacific Northwest. *Coastal Engineering*, 57, 539–552.
- Sallenger, Jr., A.H.; Karbill, W.B.; Swift, R.N.; Brock, J.; List, J.; Hansen, M.; Holman, R.A.; Manizade, S.; Sontag, J.; Meredith, A.; Morgan, K.; Yunkel, J.K.; Fredrick, E.B., and Stockdon, H., 2003. Evaluation of airborne topographic LiDAR for quantifying beach changes. *Journal of Coastal Research*, 19(1), 125–133.
- Seymour, R.J., 2011. Evidence for changes to the northwest Pacific wave climate. *Journal of Coastal Research*, 27(1), 194–201.
- Shih, S.M. and Komar, P.D., 1994. Sediments, beach morphology and sea cliff erosion within an Oregon coast littoral cell. *Journal of Coastal Research*, 10(1), 144–157.
- Sklavdis, A.I. and Lima-Blanco, W.R., 1985. Coastal Erosion along Monterey Bay. Monterey, California: Naval Postgraduate School, Master's thesis, 108p.
- Stockdon, H.F.; Sallenger, Jr., A.H.; List, J.H., and Holman, R.A., 2002. Estimation of shoreline position and change using airborne topographic lidar data. *Journal of Coastal Research*, 18(3), 502–513.
- Storlazzi, C.D. and Griggs, G.B., 2000. Influence of El Niño-Southern Oscillation (ENSO) events on the evolution of central California's shoreline. *Geological Society of America Bulletin*, 112(2), 236–249.
- Storlazzi, C.D. and Wingfield, D.K., 2005. The Spatial and Temporal Variations in Oceanographic and Meteorologic Forcing along the Central California Coast, 1980–2002: *United States Geological Survey Scientific Investigations Report 2005-5085*, 45p.
- Thieler, E.R.; Himmelstoss, E.A.; Zichichi, J.L., and Ergul, A., 2009. Digital Shoreline Analysis System (DSAS) Version 4.0—An ArcGIS Extension for Calculating Shoreline Change: *United States Geological Survey Open-File Report 2008-1278*. <http://pubs.usgs.gov/of/2008/1278/>.
- Thornton, E.B.; MacMahan, J., and Sallenger, Jr., A.H., 2007. Rip currents, mega-cusps and eroding dunes. *Marine Geology*, 240, 151–167.
- Thornton, E.B.; Sallenger, A.; Sesto, J.C.; Egley, L.; McGee, T., and Parsons, R., 2006. Sand mining impacts on long-term dune erosion in southern Monterey Bay. *Marine Geology*, 229, 45–58.
- Varekamp, J.C.; Thomas, E., and Van de Plassche, O., 1992. Relative sea-level rise and climate change over the past 1500 years. *Terra Nova*, 4, 293–304.
- Wagner, D.L.; Greene, G.H., and Saucedo, G.J., 2002. *Geologic Map of the Monterey 30'×60' Quadrangle and Adjacent Areas*. California: United States Geological Survey, Scale 1:100,000, 1 sheet.
- Zhang, K.; Douglas, B.C., and Leatherman, S.P., 2004. Global warming and coastal erosion. *Climate Change*, 64, 41–58.